

A POD-TANN approach for the multiscale modeling of materials and macroelement derivation in geomechanics

Giovanni Piunno^a, Ioannis Stefanou^b, Cristina Jommi^a

^a*Department of Civil and Environmental Engineering, Politecnico di Milano, Piazza leonardo da Vinci, 32, Milan, 20133, Italy, Italy*

^b*Nantes Université, Ecole Centrale Nantes, CNRS, Institut de Recherche en Génie Civil et Mécanique (GeM), 1 rue de la Noë BP 92101, Nantes, 44321, Pays de la Loire, France*

Abstract

This paper introduces a novel approach that combines Proper Orthogonal Decomposition (POD) with Thermodynamics-based Artificial Neural Networks (TANN) to capture the macroscopic behavior of complex inelastic systems and derive macroelements in geomechanics.

The methodology leverages POD to extract macroscopic Internal State Variables (ISVs) from microscopic state information, thereby enriching the macroscopic state description used to train an energy potential network within the TANN framework. The thermodynamic consistency provided by TANN, combined with the hierarchical nature of POD, allows for accurate modeling of complex, non-linear material behavior and reliable macroscopic geomechanical systems responses.

The effectiveness of this approach is validated through applications of increasing complexity, demonstrating its capability to handle various material behaviors and microstructural topologies. These applications include the homogenization of continuous inelastic representative unit cells (RUCs) and the derivation of a macroelement for a geotechnical system involving a monopile in a clay layer subjected to horizontal loading.

The results indicate that the proposed POD-TANN methodology not only achieves high accuracy in reproducing stress-strain responses, but also significantly reduces computational costs, making it a practical tool for the multi-scale modeling of heterogeneous inelastic systems, and the efficient derivation of macroelements for complex geomechanical problems.

Keywords: POD, TANN, Multiscale, Macroelement, Geomechanics, ROM

1. Introduction

The study of matter through multi-scale analysis has revealed that what appears homogeneous at the macroscopic level is actually composed of numerous interacting components at the microscopic level, giving rise to various macroscopic effects. Historically, engineering approaches have simplified the description of the macroscopic behavior of complex systems, often relying on phenomenological models that replicate experimentally observed behaviors. While successful, these models fail to account for microscopic processes and interactions, limiting their accuracy and predictive capability.

There are two main challenges in establishing a machine learning (ML)-based homogenization procedure. First, the obtained model at the macroscale must comply with basic physical laws, a general requirement not specific to ML techniques adopted to derive it. This necessitates incorporating such laws into the structure of the ML tools. Recently, neural network-based approaches have been proposed that incorporate basic physical laws into the model structure by design (see [1], [2], [3], [4], among others). Second, the multi-scale problem must account for the properties and responses of the constituents at the microscopic level. Examples of ML-based strategies for accelerating multi-scale analyses can be found in [5], [6].

Resolving the coupled problem described above is an open and active research topic. In this study, a Thermodynamics-based Artificial Neural Networks (TANN) formulation [7], [8], [9] is adopted, and a new and more systematic method for identifying the Internal State Variables (ISVs) of microstructured inelastic systems is proposed, based on Proper Orthogonal Decomposition (POD). Specifically, POD is integrated into the TANN workflow to learn the energy potential of the macroscopic homogenized system.

Traditionally, POD has been used to extract the dominant spatial patterns (modes) of a high-dimensional system by performing a singular value decomposition (SVD) on the snapshot matrix of the system's state variables. The resulting modes are then used to construct a low-dimensional Reduced Order Model for the system by projecting the PDEs describing the system's evolution onto the modes and solving the reduced equations using Galerkin methods [10], [11], [12], [13], [14].

In this work, POD is applied to a set of microscopic state variables to extract the internal state variables at the macroscopic scale as a result of

dimensionality reduction. Unlike other techniques, POD offers an unsupervised identification methodology that is hierarchical, preserving maximal information in the reduced space given the dimension of the embedding. This feature is exploited in the paper to select a sufficiently large space of ISVs for training the energy network, a neural network used to learn the macroscopic (Helmholtz) free energy of the composite.

The hierarchical nature of POD, along with its robustness and efficiency, significantly reduces the computational cost by decoupling the ISV identification from the training of the energy network.

The proposed method bears some similarities to the analytical Nonuniform Transformation Field Analysis (NTFA) method by Michel and Suquet [15], [16], [17], [18], based on the pioneering work of Dvorak [19]. The NTFA theory focuses on composites made of Generalized Standard Materials (GSM), as defined by [20], and aims to determine the reduced potentials of the composite, i.e., those describing the macroscopic effective behavior, from the knowledge of the constituent models [21]. At the core of the NTFA approach, similar to what is proposed in this paper, is the selection of a reduced basis to perform a model reduction of the local internal variables of the nonlinear constituents by projection. However, unlike the NTFA method, the methodology proposed here can address a more general class of materials and provides a unified workflow to derive the homogenized model, relying on the combined use of POD and thermodynamics-based artificial neural networks.

POD is also used as a practical and efficient tool for bridging the micro- and macro scales bidirectionally. In the upscaling direction, it characterizes the macroscopic state from microscopic information. In the downscaling direction, POD reconstructs the microscopic fields with a given accuracy defined by the reconstruction error. The modes used for projection (upward) and reconstruction (downward) are computed in a pre-processing step once and for all, prior to the training of the TANN energy network. This approach is extremely time-saving compared to alternative methods like autoencoders used in [8], which require coupled training with the TANN network each time.

The examples of applications presented in this study are of two types. First, the multi-scale homogenization problem of elasto-plastic heterogeneous materials with continuous microstructure is addressed. Second, the same POD-TANN framework is used to derive a macroelement featuring a single degree of freedom from a complex three-dimensional FE model of a geotechnical system. This latter example is focused on a monopile in a clay layer

subjected to horizontal loading.

The paper is divided into four sections. Section 2 reviews the theoretical framework. In Section 3, TANNs are discussed, and the proposed POD-TANN approach is outlined, starting with a brief review of the POD method to explain its use for the multi-scale problem. Section 4 presents applications of the methodology. Section 5 offers the conclusions drawn from the research.

2. Theoretical background

Constitutive equations maps system-specific responses to a given set of external actions under a given set of constraints. In continuum mechanics, constitutive equations also have a precise role in the mathematical formulations of the system of differential field equations of the studied body. Due to the unbalanced number of unknown fields, which is larger than the number of field equations derived from balance and conservation laws, the latter describing the physics of the problem, constitutive equations are needed to achieve the closure of the system.

Here the thermodynamic framework introduced by Coleman and Gurtin [22] is considered, which provides the necessary mathematical formalism for the constitutive description of a large class of materials (see [23] for an extensive review).

Coleman and Gurtin have based their formulation on the definition of a state spaces, $\mathcal{S}(t)$, including basic quantities, such as the strains or stresses, enriched with an additional set of Internal State Variable (*ISVs*), defined at the current time t , denoted by \mathbf{z} . The ISVs evolve according to a set of additional equations, called evolution laws.

At the core of the Coleman and Gurtin's approach is the use of the second law, in the form of the Clausius-Duhem inequality. This is exploited, together with the first law, to obtain restrictions on the form of the constitutive equations. A general review of the theory may be found in [7]. For the sake of simplicity, isothermal processes and infinitesimal strain regime will be considered in this work. The relevant quantities are introduced as follows: $\boldsymbol{\epsilon} = \text{Sym}(\nabla \mathbf{u})$, $p^{in} = \boldsymbol{\sigma} : \dot{\boldsymbol{\epsilon}}$, with \mathbf{u} being the displacement field, $\boldsymbol{\sigma}$ the Cauchy stress tensor, $\boldsymbol{\epsilon}$ the infinitesimal strain tensor, p^{in} the internal power, ∇ the gradient operator and $\text{Sym}(\bullet)$ the symmetric part operator.

In this simplified setting, the thermodynamic restrictions derived from

the exploited Clausius-Duhem inequality are provided as follows:

$$\begin{aligned}
(I \quad \text{Law}) \quad & p^{in} = \dot{\psi} + d; \\
(II \quad \text{Law}) \quad & d \geq 0; \\
(\text{Constraints}) \quad & \boldsymbol{\sigma} - \frac{\partial \hat{\psi}}{\partial \boldsymbol{\epsilon}} = 0, \quad d = -\frac{\partial \hat{\psi}}{\partial \dot{\mathbf{z}}} \cdot \dot{\mathbf{z}} \geq 0.
\end{aligned} \tag{1}$$

In the above expressions, $\psi = \hat{\psi}(\boldsymbol{\epsilon}, \mathbf{z})$ is the Helmholtz free energy density, d is the rate of mechanical dissipation. Furthermore, depending on the setting chosen by the modeler, Fenchel-Legendre transformations of the potential energy density are introduced so to switch from dependent and independent static and kinematic variables. To aid the formulation used in the following sections, the transform between the Helmholtz and Gibbs free energy densities is recalled:

$$\begin{aligned}
\psi - \phi &= \boldsymbol{\sigma} : \boldsymbol{\epsilon}; \\
\boldsymbol{\epsilon} + \frac{\partial \hat{\phi}}{\partial \boldsymbol{\sigma}} &= 0, \quad d = -\frac{\partial \hat{\phi}}{\partial \dot{\mathbf{z}}} \cdot \dot{\mathbf{z}} \geq 0;
\end{aligned} \tag{2}$$

where $\phi = \hat{\phi}(\boldsymbol{\sigma}, \mathbf{z})$ has been introduced for the Gibbs free energy density.

2.1. Formulation for multiscale homogenization problems

The formal derivation of the constitutive restrictions obtained in [22] is retained when a macroscopic constitutive equation is derived by homogenization of a microscopic system under prescribed boundary conditions. This has been demonstrated in [8], considering the framework of the asymptotic (expansion) homogenization (AEH) theory, in incremental formulation, see, e.g., [24], [25], [26].

The theory considers an heterogeneous body \mathcal{B} , with volume Ω , characterized by a microstructure made of a spatially periodic distribution of a Representative Unit Cell (RUC), with volume \mathcal{Y} . The average value of a quantity in \mathcal{Y} is denoted as:

$$\langle \bullet \rangle = \frac{1}{|\mathcal{Y}|} \int_{\mathcal{Y}} (\bullet) d\mathbf{y}, \tag{3}$$

where any point in the RUC is localized using the local coordinate vector \mathbf{y} , while the RUC is macroscopically localized in the body \mathcal{B} by the macroscopic coordinate vector \mathbf{x} .

All the fields in Ω show \mathcal{Y} -periodicity, see [26]. This property is indicated with the superscript \bullet^e . From the solution of the auxiliary problem on the RUC (see [24]), subjected to periodic displacements and anti-periodic traction vectors, the volume average macroscopic stress increments resulting from the imposed macroscopic strain increments can be found. Constitutive equations linking independent and dependent state variables at the macroscale, as the macroscopic stress and strain, still have to satisfy thermodynamic restrictions introduced in equations 1. Therefore, the volume averaged expressions of the first and second laws at the macroscopic level can be obtained, and are valid for any material point of the homogenized body \mathcal{B}_H . The expressions are formally identical to those reported in equation 1 and, exploiting the Coleman and Gurtin's procedure, lead to following macroscopic restrictions:

$$\boldsymbol{\Sigma} - \frac{\partial \hat{\Psi}}{\partial \mathbf{E}} = 0, \quad D = -\frac{\partial \hat{\Psi}}{\partial \mathbf{Z}} \cdot \dot{\mathbf{Z}} \geq 0. \quad (4)$$

in which the following volume average quantities are defined: the macroscopic Cauchy stress tensor, $\boldsymbol{\Sigma}(\mathbf{x}) \triangleq \langle \boldsymbol{\sigma}^e(\mathbf{x}, \mathbf{y}) \rangle$, the macroscopic small strain tensor $\mathbf{E}(\mathbf{x}, \mathbf{y}) \triangleq \langle \boldsymbol{\epsilon}^e(\mathbf{x}, \mathbf{y}) \rangle$, the macroscopic Helmholtz free energy density $\Psi(\mathbf{x}, \mathbf{y}) \triangleq \langle \psi^e(\mathbf{x}, \mathbf{y}) \rangle$, the macroscopic rate of mechanical dissipation $D(\mathbf{x}, \mathbf{y}) \triangleq \langle d^e(\mathbf{x}, \mathbf{y}) \rangle$, the macroscopic vector of internal state variables \mathbf{Z} .

2.2. Formulation for macroelement definition

In the previous sections, strategies were discussed for modeling the mechanical behavior of materials and obtaining a homogenized representation of the behavior of heterogeneous microstructured media, such as those typically encountered in geotechnics. However, in geotechnical engineering, it is challenging to distinguish the behavior of a macroscopic system, such as soil or a natural deposit, from that of the anthropogenic structures interacting with it. In other words, it is often necessary to study what is commonly referred to as soil-structure interaction (SSI).

SSI problems remain an unresolved issue in many geotechnical applications and pose a significant challenge for designers, as standard design approaches struggle to address such complex and multiscale problems. Moreover, commercial numerical codes, although increasingly accurate, often demand substantial computational resources and advanced theoretical knowledge, making them impractical as standard design tools, particularly in the preliminary stages of the design process.

In this context, where direct and time-efficient applicability to real engineering problems is crucial, macroelement approaches frequently offer a viable alternative modeling option. The key is to describe the SSI in terms of generalized stress and strain variables. This involves lumping stress variables, such as vertical and horizontal forces or moments, and soil strain fields into kinematic variables, representing structural displacements or rotations relative to the far-field boundary.

Macroelements allow for the problem to be upscaled from the local scale where numerical integration over the spatial domain is required, provided a proper constitutive relationship is assigned to each representative elementary volume or unit cell, equilibrium and compatibility equations are satisfied, and boundary and initial conditions are specified to the macro scale of the structure and its surrounding soil. In other words, an ad hoc “generalized” constitutive relationship is introduced, relating the aforementioned generalized stress and strain variables. The structure and the interacting soil are then considered as a single “macro” element, whose behavior is fully described by a limited number of degrees of freedom [27].

The important advantage of the macroelement approach is the possibility of exploiting pre-existing mechanical and thermodynamical theories defined at the local material scale to the scale of the whole engineering system, introducing a certain degree of empiricism in the modeler choice of the set of generalized static and kinematic variables. By denoting with \mathbf{F} and \mathbf{u} the work-conjugate set of generalized forces and displacements, the first principle can be written as follows:

$$\dot{f} = \mathbf{F} \cdot \dot{\mathbf{u}} - D, \quad (5)$$

having introduced the Helmholtz energy of the system, f . Using the same arguments mentioned above and exploiting the Legendre transform to formulate the problem using the force-driven Gibbs energy, $g = \hat{g}(\mathbf{F}, \mathbf{Z})$, the thermodynamic restriction of the constitutive model of the macro system can be written as follows:

$$\mathbf{u} - \frac{\partial \hat{g}}{\partial \mathbf{F}} = 0, \quad D = -\frac{\partial \hat{g}}{\partial \mathbf{Z}} \cdot \dot{\mathbf{Z}} \geq 0, \quad (6)$$

where for the mechanical rate of dissipation and the set of macroscopic internal state variables, the symbols D and \mathbf{Z} have been used, in analogy to what done for the rate of dissipation and ISV vector of the homogenized RUC.

3. Thermodynamic-based Artificial Neural Networks for the multiscale problem

Relying on the theoretical background presented in Section 2, Masi et al. [7] have developed the so called Thermodynamics-based Artificial Neural Networks - TANN, to learn the constitutive behavior of inelastic homogeneous materials. The initial TANN formulation has been further extended from homogeneity, to discrete heterogeneous micro-structured inelastic materials in [8].

At the core of the Coleman and Gurtin's theory is the learning of two functions: the Helmholtz free energy density function and the evolution law of the internal state variables. Therefore, the TANN consists of two networks: one is used to learn the potential energy function from data; the second one is used to learn the evolution law from data. The balance of energy in 1 is imposed during training by construction, differentiating the energy network's output with respect to its strain input, so to get the stress tensor exploiting auto-differentiation, see [28]. The non-negativeness of the rate of mechanical dissipation is learned from data. This is achieved including in the loss function of the energy network a regularization term in the rate of dissipation.

More specifically, the energy network inputs are the state of the material \mathcal{S} at time t , namely $\boldsymbol{\epsilon}(t)$, $\mathbf{z}(t)$. The TANN is trained to output the Helmholtz free-energy at time t , $\psi = f^\psi(\mathcal{S})$. The stress at time t is obtained as the partial derivative of f^ψ with respect to the infinitesimal strains, $\boldsymbol{\sigma} = \partial_{\boldsymbol{\epsilon}} f^\psi$, and the mechanical dissipation rate as follows, $d = -\partial_{\mathbf{z}} f^\psi \cdot \dot{\mathbf{z}}$. The regularization term is included in the training loss to penalize negative predictions of the rate of dissipation. It is defined as $\{d\} = \text{Relu}(-(-\partial_{\mathbf{z}} f^\psi \cdot \dot{\mathbf{z}}))$, with $\text{Relu}(\bullet) = \{\bullet, \text{ if } \bullet > 0; 0, \text{ otherwise}\}$.

The loss function, \mathcal{L} , is therefore the sum of four weighted terms:

$$\mathcal{L} = w^\psi \ell^\psi + w^\sigma \ell^\sigma + w^d \ell^d + w^{\{d\}} \ell^{\{d\}}. \quad (7)$$

The weights, w^i with i in $[\psi, \sigma, d, \{d\}]$, are used to assess the relative output influence on the training process; the training losses, ℓ^i , are computed using a metric of the error between the output and the training data.

3.1. Discovery of internal state variables using model reduction

Following the adopted thermodynamic framework, the energy network can be trained once the state space of the material is completely defined.

For macroscopic micro-structured systems it is not straightforward to fully characterize the state space, and defining the vector of ISV. In [8], the problem is addressed by means of dimensionality reduction techniques on the so called Internal Coordinates (IC), ξ , i.e. the set of all the quantities describing the material state at the microscopic scale.

It is remarked that *Encoding* refers to the computation of a reduced and parametrized representation of a state, whereas *Decoding* or reconstruction describes the computation of the actual state from the parametrized representation.

In [8], autoencoders are used to learn an unsupervised lower-dimensional representation of the IC, serving as the ISV vector at the macroscale. In this work, the Proper Orthogonal Decomposition (POD) is used instead as a simplified, yet effective tool for the unsupervised identification of macroscopic ISVs from a set of microscopic Internal Coordinates. The POD method can be seen as an encoder/decoder based on linear projections, thus can be recovered as a special case of an autoencoder [29]. However, several reasons motivate the use of the classical POD method in this work.

- By definition, the set of internal state variables must accurately represent the processes occurring at the microscale. However, the concept of representativeness requires careful clarification. A set of internal variables is considered representative if, in conjunction with the macroscopic strain state, it can provide a state space sufficiently large to establish a one-to-one relationship with the Helmholtz free energy density through a state function. In the context of thermodynamic-based artificial neural networks, this entails identifying a set that minimizes the loss function of the energy network to a specified threshold, while in POD is directly accessible by means of the Singular Value Decomposition of the snapshot matrix.
- The Proper Orthogonal Decomposition is a hierarchical dimensionality reduction technique designed to preserve as much information as possible within a reduced dimensional space. Achieving a predefined threshold of training loss involves increasing the number of considered POD components, ensuring the accuracy of the micro-structural processes is maintained.
- The maximum representativeness achieved through the hierarchical sorting of POD modes provides a significant advantage: it eliminates

the need to couple POD regression with the training of the energy network. In contrast, when using an encoder, the reduced dimensionality of the output does not necessarily preserve the maximum amount of information from the original set. The training of an autoencoder is only ensuring that the composition of the nonlinear mappings of the encoder and decoder results in the identity operator. This necessitates coupling the training of the encoder within the TANN workflow to ensure the thermodynamic consistency of the dimensionality reduction, as detailed in [8]. Consequently, POD, being less computationally expensive, significantly reduces the computational cost associated with training the energy network.

- The POD is a linear method that involves matrix multiplications, ensuring the existence of an inverse function. Consequently, there is no need to train an additional decoder to reconstruct the microscopic fields collected in the internal coordinates from the internal state variables vector.
- The POD algorithm is fast, robust, and efficient, and does not require the finetuning of complicated hyperparameters, as in the case of autoencoders.

In the proposed POD-TANN framework, the POD is employed to reduce the dimensionality of the internal coordinates, $\boldsymbol{\xi}$, which are responsible for tracking the irreversible processes occurring at the microscale. By applying POD to the snapshot matrix $\boldsymbol{\Xi}$, constructed from successive snapshots of $\boldsymbol{\xi}$, the ICs are approximated using a set of optimal spatial modes, $\boldsymbol{\Phi}$, and time-varying coefficients, \boldsymbol{Z} .

Mathematically, the field of internal coordinates, $\boldsymbol{\xi}$, can be expressed as:

$$\boldsymbol{\xi}(\boldsymbol{x}, t) = \sum_{k=1}^r z_k(t) \boldsymbol{\Phi}_k(\boldsymbol{x}) = \boldsymbol{\Phi}(\boldsymbol{x}) \boldsymbol{Z}(t), \quad (8)$$

where r is the number of retained POD modes, $\boldsymbol{\Phi}_k(\boldsymbol{x})$ are the time-independent spatial modes, and $\boldsymbol{Z}(t)$ is the collection of vectors of time-dependent POD coefficients, representing the reduced-order internal state variables (ISVs) at each time step.

The optimal POD basis, $\boldsymbol{\Phi}$, is derived through the Singular Value Decomposition (SVD) of the snapshot matrix $\boldsymbol{\Xi}$, which organizes the snapshots

of the internal coordinate field. Through SVD, Ξ is approximated and decomposed as:

$$\Xi \approx \tilde{\Xi} = \tilde{\mathbf{U}} \tilde{\mathbf{S}} \tilde{\mathbf{V}}^*, \quad (9)$$

where $\tilde{\mathbf{U}}$ contains the first r time-invariant spatial modes (POD modes) of \mathbf{U} , $\tilde{\mathbf{S}}$ holds the retained singular values, and $\tilde{\mathbf{V}}^*$ contains the time coefficients, with $*$ indicating the transposed-conjugate. By retaining only the dominant r modes, the dimensionality of the ICs is reduced, yielding a compact yet representative set of ISVs, \mathbf{Z} , that describe the system's evolution. \mathbf{Z} is obtained projecting ξ onto the basis defined by the orthogonal retained modes, namely $\mathbf{Z} = \tilde{\mathbf{U}}^* \xi$ (see Appendix A for a detailed derivation). Exploiting the time-invariance of the POD-modes, the rate of change of the ISV are also easily found from the rate of change of the ICs, as follows:

$$\dot{\mathbf{Z}} = \frac{d}{dt}(\tilde{\mathbf{U}}^* \xi) = \tilde{\mathbf{U}}^* \dot{\xi}. \quad (10)$$

3.1.1. State definition for the homogenization problem

The integration of the POD within the TANN framework is achieved performing the SVD onto a snapshot matrix of the IC, resulting from the collection of the strain paths used to create a database. Once the eigenbasis is found, the ISV vector is simply found by projection of the IC onto the POD modes. Considering the macroscopic state of the homogenized continuum, described in section 2.1, the following can be written:

$$\mathcal{S} = [\mathbf{E}, \mathbf{Z}] = \left[\mathbf{E}, \tilde{\mathbf{U}}^* \xi \right]. \quad (11)$$

Eventually, the TANN workflow can be used without any modification at the macroscale, once the above defined volume averaged quantities are considered. Figure 1 shows a sketch of the energy network's architecture at the macroscale, adopted in section 4.

3.1.2. State definition for the macroelement

Adopting an equivalent approach on a snapshot matrix of the IC of the macroscopic system, the state space for the macroelement can be defined as follows:

$$\mathcal{S} = [\mathbf{U}, \mathbf{Z}] = \left[\mathbf{U}, \tilde{\mathbf{U}}^* \xi \right], \quad (12)$$

or, alternatively:

$$\mathcal{S} = [\mathbf{F}, \mathbf{Z}] = \left[\mathbf{F}, \tilde{\mathbf{U}}^* \xi \right], \quad (13)$$

depending if a force- or displacement-based approach is adopted.

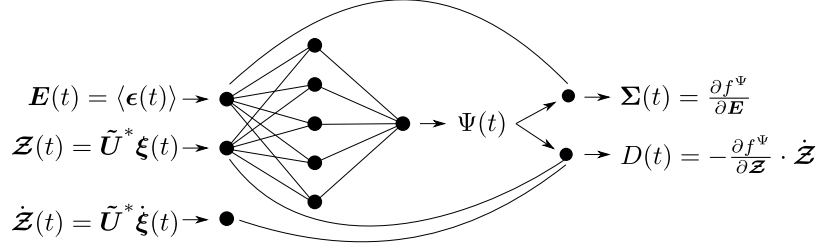


Figure 1: Sketch of the energy network of the POD-aided TANN used for the discovery of the macroscopic Helmholtz free energy density function of the homogenized micro-structured medium.

3.2. Energy reconstruction error

The ability to decouple energy network training from the identification of the internal state variables (ISV) is attributed to the hierarchical nature of the Proper Orthogonal Decomposition (POD). However, determining the exact number of POD modes required for a low-rank approximation of ξ is not straightforward. This necessitates exploring the possibility of identifying a sufficient number of POD modes that can ensure the training of the energy network meets a predetermined error bound.

In practical applications, the number of retained POD modes is typically chosen based on a threshold for the cumulative sum of the normalized singular values, usually set at 0.95 or higher. However, this choice often lacks a solid theoretical justification [12]. In this context, [30] have proposed a mathematical procedure to determine the optimal hard threshold for SVD truncation, assuming that the high-rank matrix has a low-rank structure contaminated with Gaussian white noise.

This work adopts a different approach. In particular, the number of POD modes is chosen by requiring a predefined error tolerance between the exact, Ψ , and the reconstructed, $\bar{\Psi}$, free energy of the system.

Starting from the vector of collected IC, ξ , it is possible to apply the SVD and compute a reconstructed IC vector, $\bar{\xi} = \bar{U}\bar{U}^*\xi = \bar{U}\bar{S}\bar{V}^*$, function of the given number of POD modes considered. From $\bar{\xi}$, the field of microscopic reconstructed Helmholtz energy can be obtained and, in turn, the reconstructed macroscopic energy. Namely, the reconstructed macroscopic energy, $\bar{\Psi}$, can be written as follows:

$$\bar{\Psi} = \mathcal{O}(\bar{\psi}) = \mathcal{O}(f^\psi(\bar{\xi})) = \mathcal{O}(f^\psi(\bar{U}\bar{U}^*\xi)), \quad (14)$$

where \mathcal{O} is an appropriate upscaling operator, like the volume average, $\langle \bullet \rangle$, in the homogenization problem. $\bar{\Psi}$ is therefore a function of the number of POD modes considered, N_{POD} , and can be exploited to define a reconstruction error on a normalized macroscopic energy:

$$err_{\Psi}(t) = \frac{\Psi(t) - \bar{\Psi}(t)}{\Psi_{mean}}, \quad (15)$$

where Ψ_{mean} is the mean value of the energy data in the dataset among all the possible values at any time. Thus, err_{Ψ} is quantifying how high the reconstruction error is relative to the mean of the energy values in the dataset. It is remarked that the energy is defined with respect to a reference value, which, in this case, has been taken to 0 for the undeformed configuration.

Based on the reconstruction error as a function of the number of retained POD modes, it is feasible to select an optimal number, N_{POD} , that ensures the reconstruction of the Helmholtz free energy at the macroscale is within a predefined threshold. Intriguingly and logically, this threshold for energy reconstruction is mirrored in the converging values of the loss function observed in the training learning curves of the energy network, NN^{Ψ} . This phenomenon is elucidated as follows: the internal state variables vector, \mathbf{Z} , serves as an input to the energy network. The extent of microscopic information it contains is directly proportional to the number of retained POD modes. Consequently, with a fixed number of POD modes, the macroscopic energy reconstruction error can be quantified, delineating the upper limit of what the energy network can learn. It is unrealistic to expect the network to assimilate more precise information than what is inherent in the data.

Based on the reconstruction error as a function of the number of retained POD modes, an optimal number, N_{POD} , can be selected to ensure the Helmholtz free energy reconstruction at the macroscale remains within a predefined threshold. This threshold aligns with the converging values of the loss function in the energy network, NN^{Ψ} , indicating the extent of microscopic information captured by the retained POD modes.

The advantage offered by this procedure is the a priori estimation of the attainable training error of the energy network. This allows for an informed decision on the number of POD modes to retain, ensuring efficient and effective training of the network.

When it is not possible to calculate the energy at the microscale, the benefit of a priori error estimation is lost. Nevertheless, the number of retained POD modes can be introduced as an additional hyperparameter to

regulate the overall loss reduction. By adjusting the number of POD modes, the neural network can achieve a progressively smaller training error until it reaches an asymptotic value, at which point the benefit of increasing the retained POD modes is outweighed by the increased computational time due to the network's complexity. However, this procedure is beyond the scope of this work and is reserved for future research.

3.3. Uniqueness of the energy functions

The energy network undergoes a supervised training process in which data of energy, stress and rate of dissipation have to be provided. As already pointed out in [9], [31], it is not strictly necessary to include the output of the energy in the trainable variables, since compliance with the first law is guaranteed by construction, regardless of the accuracy of the energy data reproduction. In the following, the possibility of eliminating the rate of dissipation data is also taken into account.

A first consideration to make is on the uniqueness of the partition of the internal power in the first law. For isothermal processes, the first law is rewritten as follows: $\boldsymbol{\sigma} : \dot{\boldsymbol{\epsilon}} = \dot{\psi} + d$, in which it is seen that the internal power is partitioned into the rate of stored energy and the rate of dissipated energy. Collins and Houlsby [32], have remarked that the decomposition is in general not unique. To show this, we assume to define a constitutive model by means of the two functions Helmholtz free energy density $\psi_1 = f_1^\psi(\boldsymbol{\epsilon}, \mathbf{z})$ and rate of dissipation d_1 . An additional model is considered, characterized by $\psi_2 = f_1^\psi(\boldsymbol{\epsilon}, \mathbf{z}) + f_2^\psi(\mathbf{z})$ and d_2 . Substituting the functions defining the two models within the first law, the following expressions are found:

$$\begin{aligned}\dot{\psi}_1 &= \frac{\partial f_1^\psi}{\partial \boldsymbol{\epsilon}} : \dot{\boldsymbol{\epsilon}} + \frac{\partial f_1^\psi}{\partial \mathbf{z}} \cdot \dot{\mathbf{z}} = \boldsymbol{\sigma} : \dot{\boldsymbol{\epsilon}} - d_1, \\ \dot{\psi}_2 &= \frac{\partial f_1^\psi}{\partial \boldsymbol{\epsilon}} : \dot{\boldsymbol{\epsilon}} + \frac{\partial f_1^\psi}{\partial \mathbf{z}} \cdot \dot{\mathbf{z}} + \frac{\partial f_2^\psi}{\partial \mathbf{z}} \cdot \dot{\mathbf{z}} = \boldsymbol{\sigma} : \dot{\boldsymbol{\epsilon}} - d_2.\end{aligned}\tag{16}$$

It is straightforward to see that the stress, which is the quantity of interest, is identical between the two models, $\boldsymbol{\sigma} = \partial f_1^\psi / \partial \boldsymbol{\epsilon} = \partial f_2^\psi / \partial \boldsymbol{\epsilon}$, even though the free energy model is different, as well as the rate of mechanical dissipation, that results to be $d_2 = d_1 - \frac{\partial f_2^\psi}{\partial \mathbf{z}} \cdot \dot{\mathbf{z}}$.

Starting from this consideration, using both energy and dissipation rate data obtained from specific energy models could impose an unnecessary requirement during the training of the energy network. TANN can determine

an adequate energy function based solely on stress data. It is important to recall that the aim of TANN is to achieve thermodynamically admissible constitutive predictions, meaning consistent predictions of stress and state variable increments based on strain increments. Excluding the dissipation term from the training loss, specifically $\|d + \frac{NN^\Psi}{\partial \mathbf{Z}} \dot{\mathbf{Z}}\|$, would prevent the network from learning the exact rate of the dissipation model included in the data. However, it would still ensure the thermodynamic consistency of the predictions and the correct reproduction of the stress tensor.

A further benefit of excluding the energy terms in the training data is the enhanced applicability of TANN for data derived from laboratory experiments, where measuring energy quantities is often challenging.

Therefore, the following loss function will be considered:

$$\mathcal{L} = w^\sigma \ell^\sigma + w^{\{d\}} \ell^{\{d\}}. \quad (17)$$

4. Applications

This section will examine three applications of the proposed approach. Sections 4.1 and 4.2 will focus on learning the homogenized behavior of continuum microstructured periodic unit cells exhibiting inelastic behavior. Then, Section 4.3 will detail the data-driven derivation of a macroelement for the horizontal response of a monopile in a clayey layer.

4.1. RUC with ellipsoidal inclusion

The first example focuses on an RUC with an ellipsoidal inclusion. Both the matrix and inclusion follow an elasto-plastic model with isotropic hardening and the Drucker-Prager yield criterion. The material parameters are provided in Table 1.

4.1.1. Data generation

The training dataset was generated by applying random strain increments to the RUC, starting from an initial compression volumetric strain of -5e-4. This approach was chosen to avoid generating data in the positive (tensile) volumetric domain, which is rarely relevant for geomechanics applications. The strain paths were created by sampling increments from a standard normal distribution with a mean of 0.0 and a standard deviation of 5e-4. To ensure that a significant portion of the stress points fall within the plastic regime, a limit of 0.015 was imposed on the second deviatoric strain invariant.

Material	E (kPa)	ν (-)	ϕ (°)	$\tilde{\psi}$ (°)	c (kPa)	H (kPa)
Matrix	5500	0.3	32	32	10	4000
Inclusion	6500	0.3	30	30	12	3500

Table 1: Constitutive parameters used for the RUC with ellipsoidal inclusion. E the Young’s modulus, ν the Poisson’s ratio, ϕ the friction angle, $\tilde{\psi}$ the dilatancy angle, c the effective cohesion and H the hardening modulus.

Strain paths consisting of 1000 increments were considered. The initial dataset was composed of five random strain paths. The final dataset was then obtained through data augmentation. This involved rotating the second-order tensors of the microscopic stress and strain fields using a randomly sampled 3D rotation matrix, \mathbf{R} , while preserving invariant quantities such as energy. This augmentation not only reduced computational time for dataset generation but also allowed the neural network to learn objectivity from the data.

The ICs are obtained by collecting the elastic and plastic microscopic strains, along with the maximum second invariant of the plastic strains at the Gauss points of the computational model at each increment, expressed as $\boldsymbol{\xi} = [\boldsymbol{\epsilon}_i^{el}, \boldsymbol{\epsilon}_i^{pl}, J_{2,max}^{pl}]$ at all Gauss points. Since the hardening in this example is isotropic and linear, and there is no softening, $J_{2,max}^{pl}$ serves as the hardening variable (see [33]). These microscopic state variables are sufficient to fully describe the microscopic state at each Gauss point of the RUC.

With 10675 linear tetrahedral elements, the computational model is computationally expensive. A total of 138775 degrees of freedom have been collected in the IC matrix. As shown in Figure 2-b, with a number of POD coefficients greater than 13, the energy reconstruction error, as defined in section, is reduced to 1e-4.

The reduction in dimensionality of the ICs prior to training the energy network has been quantified using a compression ratio, CR , defined as follows:

$$CR = (1 - \dim(\mathbf{Z})/\dim(\boldsymbol{\xi})) \quad \% \quad (18)$$

With 25 POD modes, the compression is $CR = 99.98\%$. This substantial reduction is achievable due to the redundancy in the information contained within the set of internal coordinates. Although the material’s heterogeneity introduces variability in the strain fields, the gradients are primarily concentrated around the inclusion. Many Gauss points within the matrix, especially

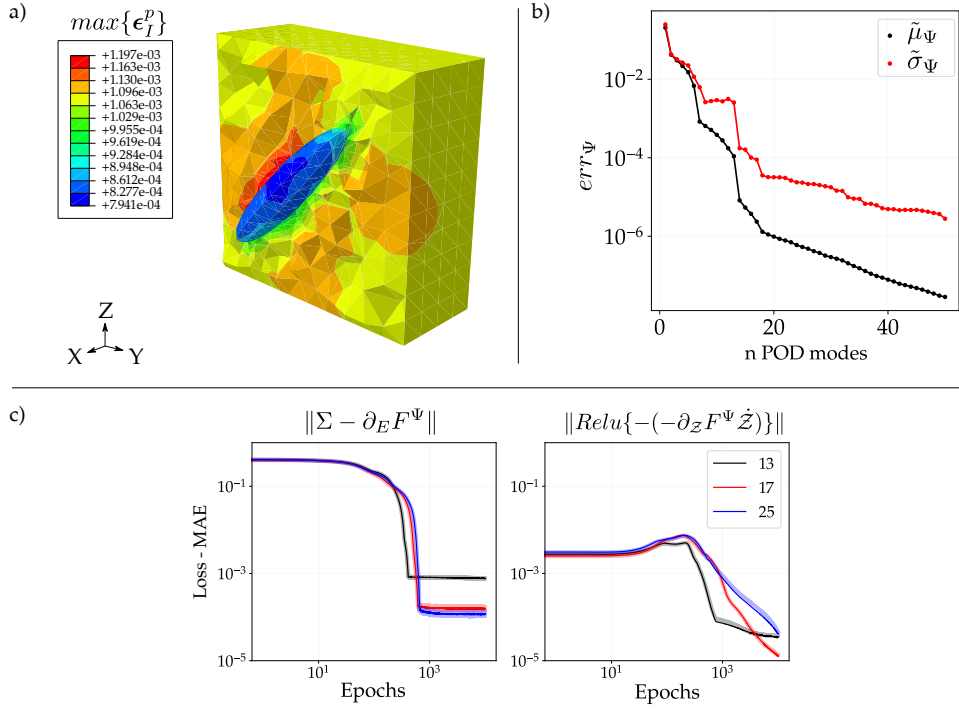


Figure 2: a) Computational model of the RUC, representation of the field of maximum principal microscopic plastic strains. b) Normalized reconstruction error $(\Psi - \tilde{\Psi})/\Psi_{max}$ of the macroscopic energy based on considered number of POD modes. $\tilde{\mu}_{\Psi}$ and $\tilde{\sigma}_{\Psi}$ are the mean and standard deviation of err_{Ψ} over all the data samples in the training set; Ψ_{max} is the maximum energy value in the training set. c) Loss curves the macroscopic stress and the regularization term on the rate of dissipation, considering 13, 17 and 25 POD modes.

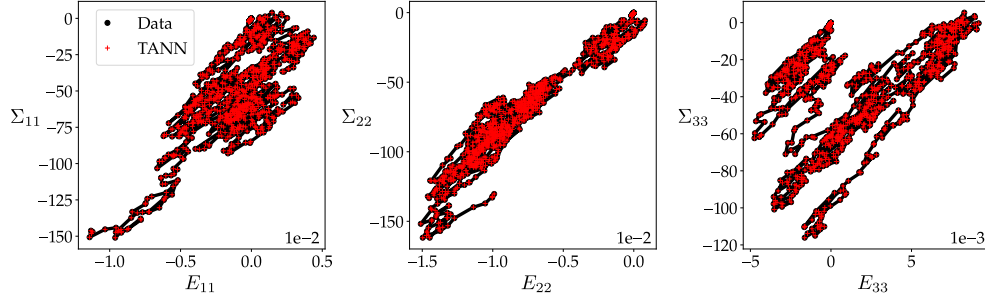


Figure 3: Prediction in inference mode of the TANN’s energy network trained considering 25 POD modes of the RUC with the ellipsoidal inclusion. The RUC is subjected to an unseen random 3D strain path. Stress components are reported as a functions of the conjugate strain components.

those far from the inclusion, exhibit strain field values that change marginally relative to one another, enabling such high compression.

4.1.2. Training of the TANN

To train the Helmholtz free energy network a supervised learning procedure has been adopted, collecting inputs and outputs as detailed in Section 3. All the inputs and outputs have been normalized to range between -1 and 1, with the exception of the Helmholtz energy and the rate of mechanical dissipation, for which positive and normalized values between 0 and 1 have been used. As schematically depicted in Figure 1, the input of the network has variable dimensionality, depending on the number of retained POD modes, in agreement with the following expression: $6 + 2 \cdot N_{POD}$. Despite the latter variability, the training of the TANN has been performed keeping constant the number of hidden layers and neurons of the energy network, as detailed below.

The energy network is a feed forward net with a single hidden layer of 100 neurons with quadratic activation function of the form $p_j^{(k)} = \mathcal{A}^k(r_j^{(k)}) = r_j^{(k)2}$, and a linear single output layer with biases set to zero. The latter guarantees the reference energy to be zero at an initial zero-valued state. The Nadam optimizer has been adopted, see [34], with a learning rate of 5e-5. Weight and biases have been initialized using the Glorot uniform initializer, see [35]. A constant mini-batch size of 1000 has been used.

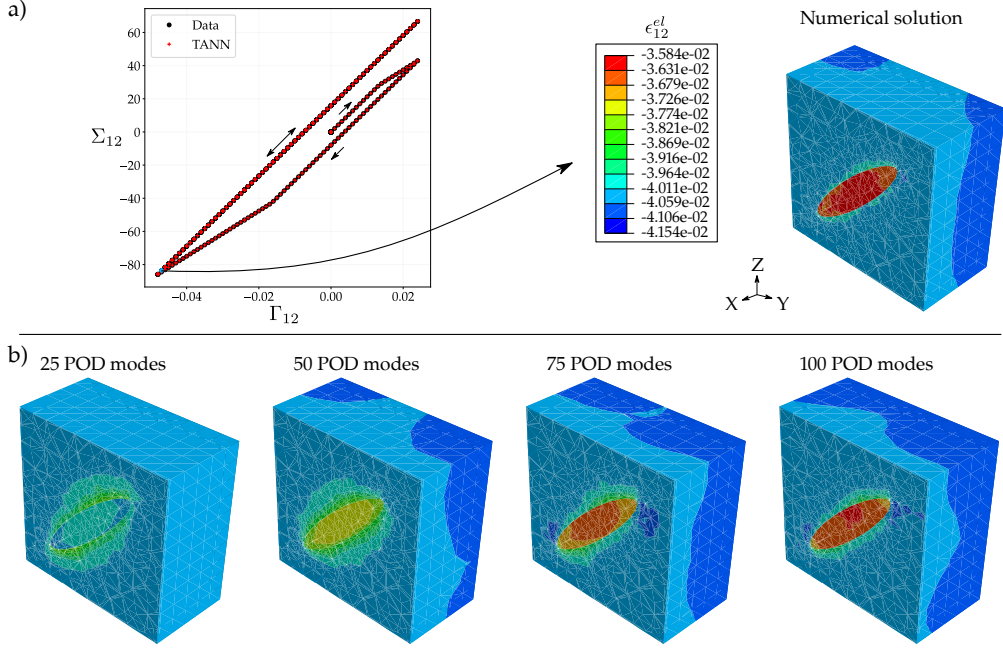


Figure 4: a) Prediction in inference mode of the TANN’s energy network trained considering 25 POD modes. On the right there is the microscopic elastic strain field corresponding to a point in the first reloading branch of the path. b) Reconstructed elastic strain field considering 25, 50, 75 and 100 POD modes.

4.1.3. Inference of the TANN

The capabilities of the trained network are tested for an unseen random 3D strain path, as reported in Figure 3. The computed Mean Absolute Error (MAE) is of the order of $1e-4$. Figure 4 illustrates the application of the TANN in inference mode along an unseen pure-shear cyclic strain-driven path, well beyond the training range. The TANN used for predictions is trained with 25 POD modes. The figure demonstrates the network’s ability to account for the evolution of internal hidden variables, successfully predicting the expansion of the elastic domain induced by isotropic hardening. Additionally, the model accurately predicts the permanent effect of hardening. After a complete stress reversal in one cycle, the expansion of the elastic domain prevents re-entering the elastic-plastic regime during subsequent cycles of the same amplitude. Consequently, the neural network predicts an elastic response along the load-unload line to the left of the origin, aligning

with the exact solution and the physics of the problem.

The use of POD enables the fast reconstruction of the detailed fields of the ICs. Figure 4-b depicts the reconstructed elastic deformation field using different numbers of POD modes. The reconstruction of the field with 25 modes achieves a MAE of approximately $1e-3$, which is satisfactory for this application. An even more accurate reconstruction of the microscopic fields can be obtained by increasing the number of POD modes; for instance, using 100 modes reduces the reconstruction MAE to $1e-5$.

The macroscopic constitutive behavior, quantified in terms of stresses, is well reproduced (with an MAE of about $1e-4$), despite the less accurate reconstruction of the microscopic fields ($1e-3$). This is naturally induced by the averaging process used to upscale the microscopic response. Therefore, depending on the application, one can choose the appropriate number of POD modes for the TANN to reconstruct the IC's fields with the required accuracy. The selection of the number of modes can be made after performing the singular value decomposition (SVD), as described in Section 3.2. The decomposition needs to be done only once, while only the energy network must be re-trained each time the selected number of POD modes changes. This is a clear advantage of our approach compared to previous ones using autoencoders ([8], [9]). Moreover, as noted in Section 3.1, autoencoders cannot provide hierarchically sorted reduced data. This implies the need to train them together with the TANN's energy network, necessitating a new, coupled training process each time the dimensionality of the reduced space is changed, which is computationally expensive.

4.2. RUC with leaf-shaped inclusion

The second example features a cubic representative unit cell (RUC) with a leaf-shaped inclusion, included to address a more complex inclusion topology. While numerous studies in the literature focus on ellipsoidal particle inclusions, such as [36], fewer explore generic geometries like the one presented in this section. This example demonstrates the versatility of the method when applied to inclusions of arbitrary shapes.

4.2.1. Data generation

The constitutive relationships for both the matrix and the inclusion are elasto-plastic, with linear isotropic hardening and the Drucker-Prager yield criterion. The constitutive parameters are detailed in Table 2. The internal configurations (ICs) used are the field variables sufficient to microscopically

Material	E (kPa)	ν (-)	ϕ ($^\circ$)	$\tilde{\psi}$ ($^\circ$)	c (kPa)	H (kPa)
Matrix	5500	0.3	25.4	25.4	5	3000
Inclusion	6500	0.3	30	30	12	2500

Table 2: Constitutive parameters used for the RUC with leaf-shaped inclusion. Symbols are defined in Table 1.

describe the state of the material, including the elastic and plastic strains and the hardening variables at the Gauss points of the finite element (FE) model. This setup results in a total of 92,703 IC degrees of freedom. The neural network is trained similarly to the previous case, with dataset augmentation by rotation. The training dataset starts with 5 sets of 1000 samples, each randomly rotated 5 times, and an initial compression volumetric strain threshold of $-5\text{e-}4$ is set for data generation.

4.2.2. Training of the TANN

The training of the TANN has been achieved using the same setting detailed in section 4.1.2. Figure 5-c presents the learning curves obtained during the training process. Remarkably, the neural network training converges after only 1000 epochs. The figure displays the learning curves for 15, 20, and 25 POD modes. A significant improvement is observed from 15 to 20 modes, with the plateau value decreasing by almost one order of magnitude. This improvement is also evident in Figure 5-b, where the average energy reconstruction error and its standard deviation decrease by approximately one order of magnitude. Beyond 20 POD modes, the error curve's slope remains nearly constant as the number of modes increases. This is reflected in the minimal difference between the stress loss curves for 20 and 25 modes, although a further decrease in the plateau value is noted with 25 modes. With 25 modes, the compression ratio is $CR = 99.97\%$.

4.2.3. Inference of the TANN

Similar to the previous cases, an example of the use of the trained network in inference mode is reported in Figure 6, to show the good reproduction of an unseen 3D random strain path.

Figure 7 illustrates another example of the use of the trained TANN's energy network in inference mode. This case reproduces a strain-driven compression triaxial test. The RUC is initially subjected to volumetric deformation, followed by simultaneous increases in the strain components E_{zz} , E_{xx}

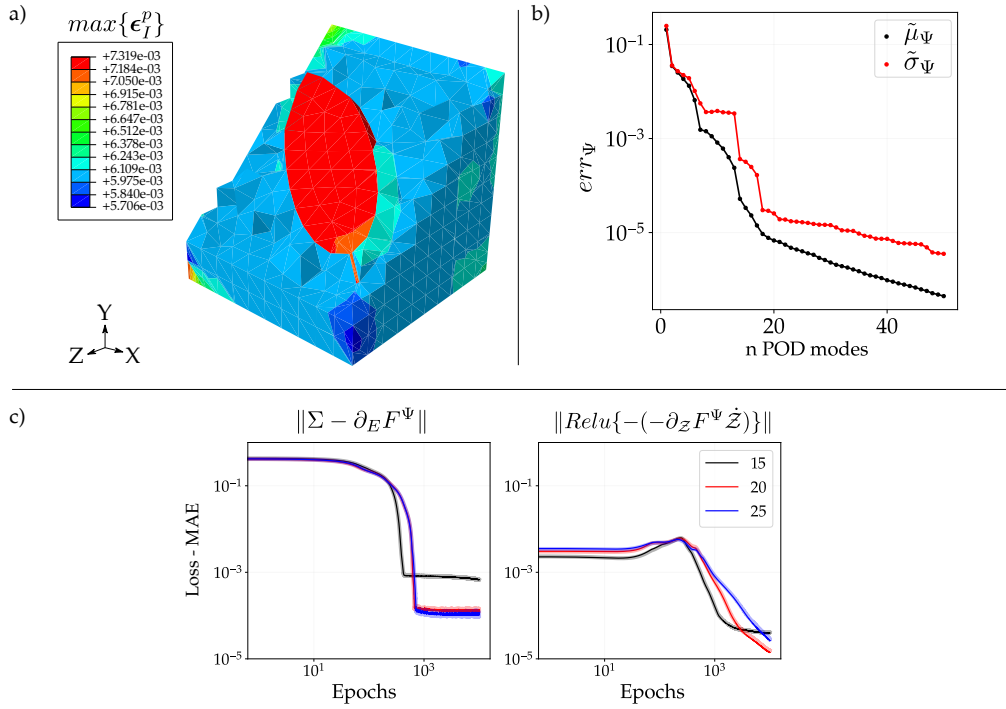


Figure 5: a) Computational model of the RUC, representation of the field of maximum principal microscopic plastic strain. b) Normalized reconstruction error $(\Psi - \tilde{\Psi})/\Psi_{max}$ of the macroscopic energy based on considered number of POD modes. $\tilde{\mu}_\Psi$ and $\tilde{\sigma}_\Psi$ are the mean and standard deviation of err_Ψ over all the data samples in the training set; Ψ_{max} is the maximum energy value in the training set. c) Loss curves of the macroscopic stress and the regularization term for imposition of the second Law, considering 15, 20 and 25 POD modes.

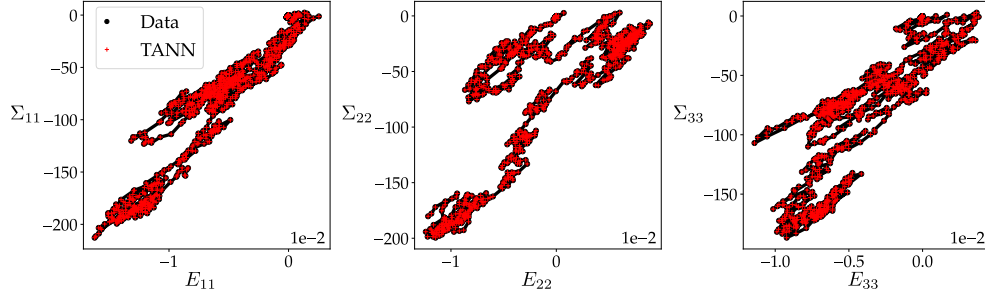


Figure 6: Example of use of the trained energy network for the RUC with leaf-shaped inclusion in inference mode. The RUC is subjected to a 3D strain driven unseen random strain path. Stress VS conjugate strain components.

and E_{yy} at a constant ratio, allowing for both volumetric and shear deformation. At the beginning of the shear phase, the stress ratio is uniquely determined by the homogenized elastic volumetric and shear stiffnesses, up to the yielding point. The first yield surface, appearing as a line in the invariant stress plane, is associated with the matrix's constitutive behavior, as shown in grey in Figure 7. The matrix elements are the first to yield. Due to stress redistribution, additional Gauss points enter the elasto-plastic regime, altering the ratio between the corresponding volumetric (still elastic) and elasto-plastic deviatoric tangent stiffnesses. This also applies to the inclusion, whose elements enter the elasto-plastic regime due to stress concentration at its boundary with the matrix. Once the matrix yields, several elements within the inclusion plastify, although its core remains elastic under the applied strain amplitude.

Figure 8 shows the microscopic plastic strain field for the first normal component at the final increment of the strain path depicted in Figure 7. The POD-reconstructed fields are compared to numerical simulation results. As anticipated, increasing the number of POD modes improves the agreement. Although the plastic field of the leaf-shaped inclusion is replicated with less accuracy, 25 modes are sufficient to capture the pattern of the major plastified zones in the matrix. The mean absolute reconstruction error is approximately $5e-4$. This error reduces to $5e-5$ when 100 POD modes are considered.

4.3. Macroelement of a monopile in saturated clay

The third example explores the possibility of utilizing the proposed POD-TANN framework to learn the energy potential of a macroelement. The focus

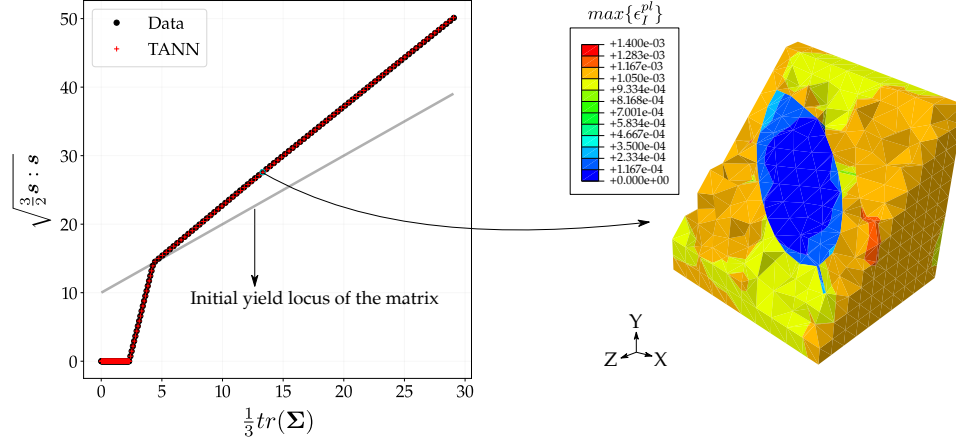


Figure 7: Example of use of the trained energy network for the RUC with leaf-shaped inclusion in inference mode. The reproduced path is a triaxial strain-driven compression test, starting from an isotropic compression.

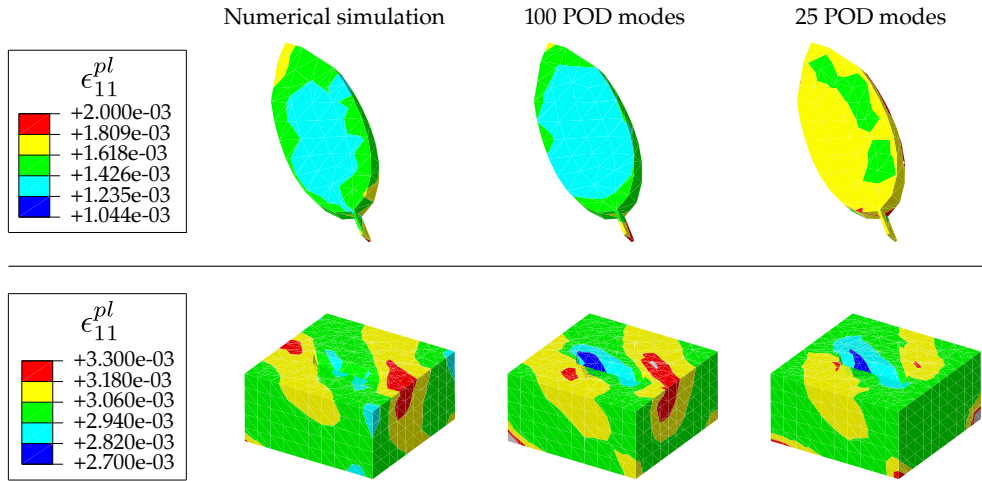


Figure 8: Reconstructed plastic strain field (ϵ_{11}^{pl} component) considering 25 and 100 POD modes. The numerical results refer to the last increment of the triaxial strain path shown in Figure 7.

is on a monopile foundation, which is the most common solution for offshore wind turbines installations in shallow waters.

Traditionally, the evaluation of the response of these types of foundations has been based on simplified approaches, such as those of p-y curves, as in [37] and [38], and more rarely on complex numerical analyses of the single pile and the foundation soil. Alternatives to these approaches are macroelements. These macroelements maintain the simplicity of use found in p-y curves, but they allow for the direct consideration of complex aspects of soil-structure interaction on the macroscopic response of the system, such as the progressive degradation of the soil's stiffness and resistance, friction between the pile and the ground, and the hysteretic damping response of the soil, among others.

In this section, a macroelement capable of replicating the horizontal undrained cyclic response in terms of force-displacement of a monopile in a saturated clay layer is presented. The macroelement results from training a TANN on a numerical database obtained from finite element simulations of the macroscopic system.

The proposed methodology utilizes the energy formulation in terms of the dual energy potential of the Helmholtz free energy, namely the Gibbs free energy. Engineering structures are often subjected to known forces, and the displacements induced by external solicitations are the unknowns. Thus, it is convenient to formulate the problem in terms of the Gibbs potential and, by its partial differentiation, obtain the horizontal displacements induced by the resultant of the external forces acting on the pile.

The TANN is combined with Proper Orthogonal Decomposition and applied to a macroscopic geotechnical system. Eventually, the studied 3D system is condensed into a macroelement with one degree of freedom.

The macroscopic state of the pile-soil system is denoted by $\mathcal{S} = [F_H, \mathbf{Z}]$, where F_H represents the resultant of the horizontal forces that are active at the pile head, and \mathbf{Z} the vector of internal state variables of the macroscopic system, which are determined based on the IC, ξ . Figure 9 illustrates a schematic representation of the procedure presented below.

In order to learn the Gibbs free energy potential function of the macroscopic system, a neural network denoted by f^Φ is trained. The network receives as input the macroscopic state of the system and returns as output the Gibbs free energy, Φ . By partial derivation of f^Φ , two further quantities are obtained: (i) the horizontal displacement, $U_H = -\frac{\partial f^\Phi}{\partial F_H}$, and the rate of mechanical dissipation, $D = -\frac{\partial f^\Phi}{\partial \mathbf{Z}} \dot{\mathbf{Z}}$.

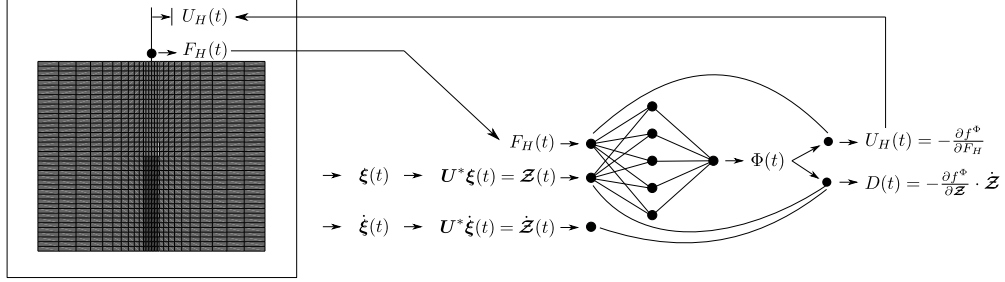


Figure 9: Schematic of the problem setting. The data obtained from the numerical FE analysis of the geotechnical system are fed into the TANN to obtain the macroscopic response of the system in terms of horizontal force-displacement.

4.3.1. Computational model

The 3D finite element model has been set up in ABAQUS [33]. To simulate the undrained response, the soil is modeled as a single-phase medium with a saturated density of $\rho_{SAT} = 2 \text{ Mg/m}^3$, and the analyses are conducted in terms of total stresses.

An elastic-plastic constitutive model with kinematic hardening and the Von-Mises yield criterion is used for the soil. The undrained resistance is a linear function of the vertical coordinate as follows: $S_u = 10 + 0.3p'(z)$, in kPa, with p' the effective mean stress. The elastic law of the soil is linear isotropic, with the Young's modulus values depending on z , as follows: $E(z) = E_{ref} \left(\frac{p'(z)}{p'_{ref}} \right)^{0.5}$, with $p'_{ref} = 30 \text{ kPa}$, $E_{ref} = 500 S_{u,ref}$, $S_{u,ref} = 20 \text{ kPa}$. The Poisson's ratio is 0.48, to account for the potential presence of gas in the saturated porous medium, thereby reducing the volumetric stiffness of the equivalent single-phase (similar to what is done for gassy soil, see [39]).

The steel pile with a hollow circular section is modeled as isotropic linear elastic with the following parameters: $E = 210 \text{ GPa}$, $\nu = 0.3$, $\rho = 7.85 \text{ Mg/m}^3$.

The soil inside the pile cavity is modeled as elastic and not elasto-plastic, with the same elastic parameters already reported. This modeling assumption is adopted following an elasto-plastic analysis, according to which it has been found the plastic deformations of the soil inside the pile to be negligible.

A Coulomb frictional contact is modeled between the pile and the soil, with a coefficient of 0.5. Figure 10 shows the dimensions of the computational model and the representation of the generated mesh.

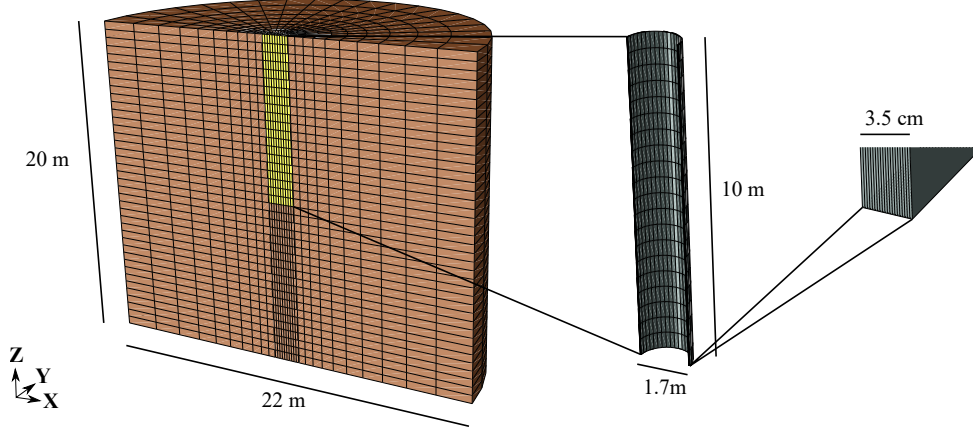


Figure 10: Computational model and generated mesh of the soil-pile system.

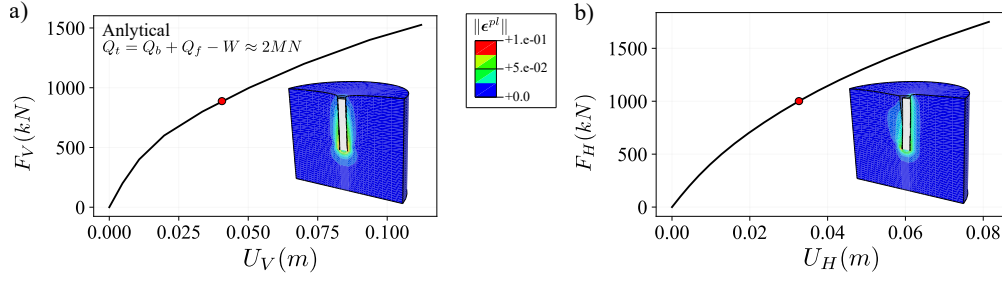


Figure 11: Monotonic load curves for vertical (a) and horizontal (b) bearing capacity.

4.3.2. Data generation and training of the TANN

The TANN training database has been obtained by subjecting the pile to a vertical operating force equal to 800 kN and to random horizontal forces variable in sign and amplitude sampled from a uniform distribution with a maximum amplitude equal to 1 MN , as highlighted by the red dots in Figure 11.

The soil-pile system is reduced to a macroelement with one degree of freedom, considering the horizontal displacement of the point at the pile head positioned on the pile axis, U_H , as a function of the resultant of the horizontal forces at the pile head, F_H .

The elastic and plastic strains, along with the hardening variable at each Gauss point of the FEM model, have been included in the IC set, onto

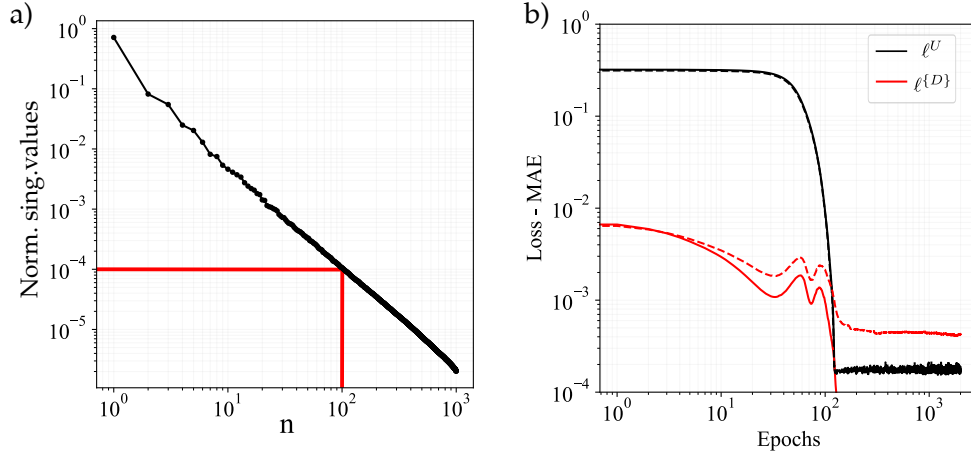


Figure 12: a) Normalized singular values obtained via POD from the set of ICs. b) Training curves of the TANN. The solid lines refer to the training set while the dotted lines refer to the validation set, used to avoid over-fitting phenomena.

which POD has been performed to obtain the ISVs. Figure 12-a displays the normalized singular values obtained. The number of POD modes retained was determined based on the relative magnitude of these normalized singular values. A threshold value of $1e-4$ was set, leading to the selection of 100 POD modes. This threshold influences directly the asymptotic value of the training losses of the TANN, as shown in Figure 12-b, where the training stopped upon reaching $1e-4$.

As already shown, the threshold of $1e-4$ allows to achieve satisfactory results both in terms of accuracy in the reproduced response of the 1D equivalent system and of the reconstruction error of the microscopic fields.

4.3.3. Inference of the TANN

For this kind of applications the possibility of reconstructing the fields used as internal coordinates is particularly appealing. One of the major drawbacks of the classical macroelement formulations is the impossibility of retrieving microscopic information, once the macroscopic behavior has been simulated. This poses clear difficulties in the engineering design, since often structural components are encapsulated by the macro-material whose response is of interest. Thus, an additional model is needed to link the global response of the classical macroelement to that of the structural components.

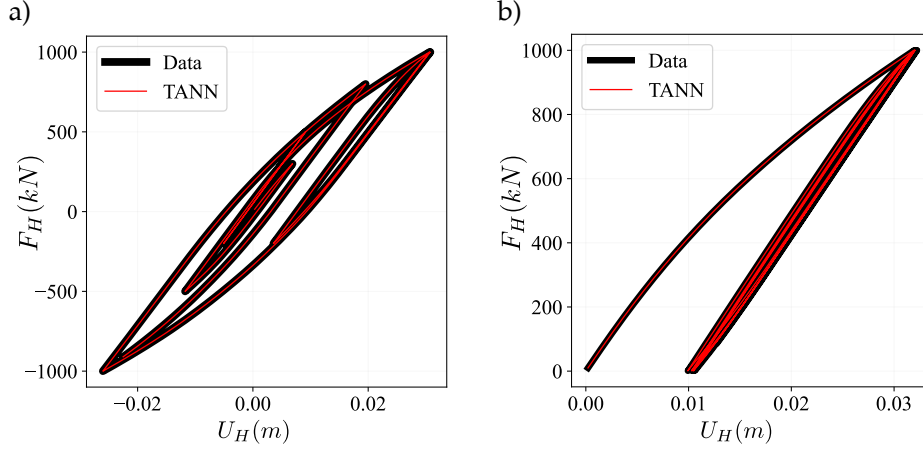


Figure 13: TANN predictions in inference of a strain path outside the training set for cycles of positive and negative amplitude (a) and asymmetric cycles (b).

As shown above, this is not needed with the proposed POD-TANN approach.

Figure 13 shows the inference responses of the trained TANN. In particular, in Figure 13-a the amplitude of the stress undergoes a total inversion between -1 and +1 MN. In Figure 13-b, an asymmetric, positive cycle is shown. The relative MAE is of the order of $1e-4$ and the displacements induced by the loading cycles are well reproduced.

The potential of the method is particularly evident for the reconstruction task. Figure 14 shows the elastic deformation field, ϵ^{el} of the pile simulated and reconstructed with the use of the POD, at the end of the last cycle of the load path of Figure 13-b.

The reconstruction error, expressed in MAE, is of the order of $1e-6$. It is remarked here that the threshold of the normalized singular values is $1e-4$, but this does not mean that the MAE of the reconstruction error has to be of the same order. The reconstruction error is computed as $\|\xi - \tilde{U}\mathbf{Z}\|$, therefore it decreases as a function of the considered POD modes, but not necessarily with the same rate.

By exploiting the known constitutive relationship, the stress field can be reconstructed with high accuracy and consequently the internal actions can be calculated for structural design.

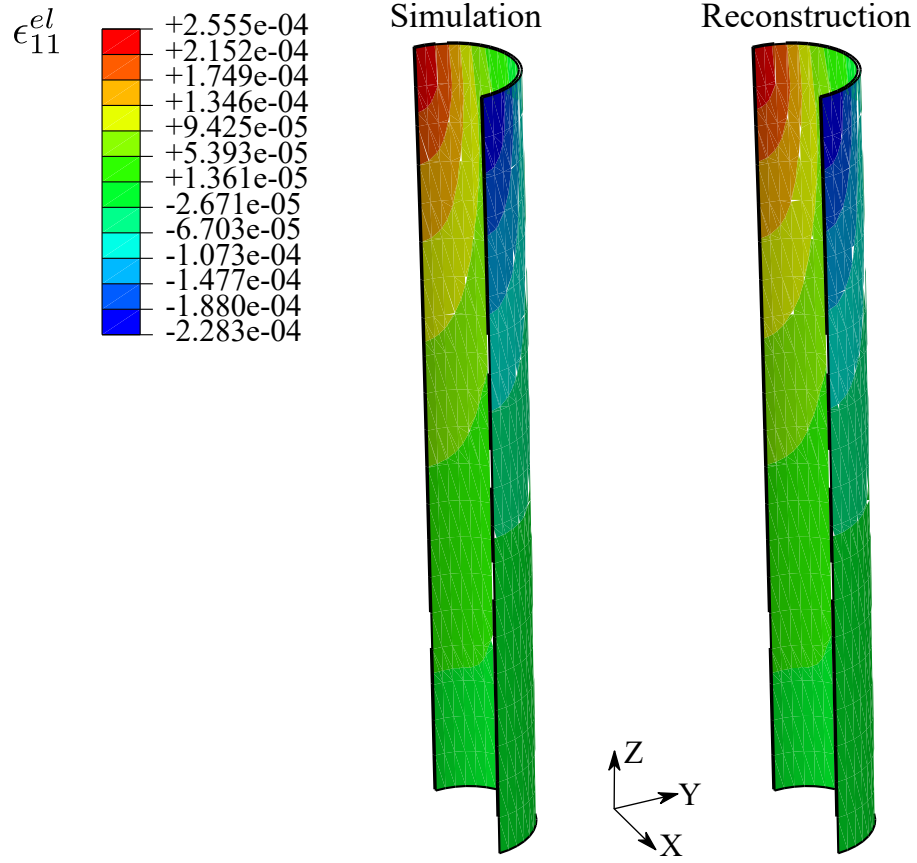


Figure 14: Comparison between the deformation field ϵ_{11}^{el} of the pile obtained from numerical simulations and reconstructed using POD.

4.3.4. Discussion on the POD-TANN macroelement calibration

The proposed application of the POD-TANN approach to macroelement derivation demonstrates the significant potential of the methodology. However, its current implementation exhibits limitations.

A primary limitation of the approach lies in its specificity. The entire procedure, encompassing the computational setup, data collection, preprocessing, and analysis, is highly tailored to the particular scenario under investigation. When the scenario changes - whether in terms of domain geometry, material properties, or boundary conditions - the entire computational process must be repeated. This also includes the task of training a new neural network, which is intrinsically linked to the specific problem it was trained on. Consequently, the approach is restricted in its ability to generalize across different scenarios of the same problems without substantial reconfiguration and retraining.

Traditionally, the calibration of macroelements in geomechanics has been rooted in the parametric formulation of these elements, aimed at reducing the need for extensive numerical computations by expressing macroelement behavior in terms of adjustable parameters functions of scenario-specific geometric data and material properties (see, e.g., [40]).

In this context, Transfer Learning (TL) presents a promising strategy to extend the applicability of the POD-TANN approach across various scenarios.

Specifically, TL could enhance the POD-TANN methodology in two significant ways:

- Fine-tuning pre-trained networks: TL allows for the adaptation of a pre-trained neural network to new scenarios, even when these scenarios differ in domain geometry or material parameters. The pre-trained network, which encapsulates the learned behavior from the original scenario, can be fine-tuned using a smaller, scenario-specific dataset. This approach significantly reduces the computational effort associated with training a new network from scratch for each new problem. This concept has been successfully demonstrated in recent studies, such as [41], where TL has been used to adapt models to different geotechnical conditions efficiently.
- Development of parametric macroelement networks: TL algorithms can be designed to link specific model input parameters, such as geometry and material properties, to each new scenario. By incorporating

these parameters into the force vector and initial conditions, it is possible to develop a parametric macroelement network. Such a network would generalize across a range of scenarios, providing a computationally efficient tool for geomechanical modeling. In this perspective, [42] demonstrated the potential of TL in parametric modeling by applying it to the stability analysis of slopes with varying spatial distributions, highlighting the achievable efficiency gain.

An important consideration in this context is the number of POD modes used in the model, as this directly influences the dimensionality of the internal state variable vector. The selection of POD modes is crucial, as it determines how well the reduced-order model can capture the essential features of the system. For TL to be effective across different scenarios, the selected number of POD modes should be representative across a range of macro-model parameters, including variations in geometry, material properties, and boundary conditions, as stated before. This requirement would ensure that the fixed number of POD modes (i.e. of ISV vector components) remains unchanged and sufficient for new scenarios, thereby enabling the successful application of TL, without TANN’s hyperparameters changes (e.g., the number of inputs, and consequently the number and density of hidden layers).

In this view, the need to maintain a consistent number of POD modes across different scenarios could serve as an additional criterion for determining the appropriate number of POD modes. Rather than solely focusing on ensuring that the learning targets are met, this approach would also consider the need to encompass a class of possible macro-model parameters, facilitating more effective TL.

This dual consideration could help balance the trade-off between model accuracy and computational efficiency while broadening the applicability of the POD-TANN approach.

5. Discussion and conclusions

A new POD-TANN methodology has been presented, which incorporates Proper Orthogonal Decomposition into the training workflow of Thermodynamics-based Artificial Neural Networks [7], for modeling the macroscopic behavior of inelastic systems with microstructure.

The POD is applied to datasets of snapshots of internal coordinates, i.e., to the set of state variables apt to describe the processes taking place

at the microscale of the investigated heterogeneous, inelastic materials. The method places at its core the hierarchical structure of the modes obtained via POD, which guarantees the maximum representativeness of the information contained in the obtained first N -th modes. The consequent hierarchical sorting of the ISV vector’s components allows decoupling the dimensionality reduction procedure from the training of the TANN network. This procedure offers great versatility. Indeed, the number of the ISV’s components can be selected based on the degree of accuracy depending on the applications.

One key benefit of this approach is the possibility of including microscopic information at the macroscale through a linear dimensionality reduction technique that is straightforward to implement, fast, and robust. The linear mapping is guaranteed to be invertible, making the reconstruction of the microscopic fields always possible. This feature is very compelling since it provides the direct and inverse mapping to perform homogenization at the macroscale and the reconstruction of the fields at the microscale, respectively. However, this feature is influenced by the number of POD modes considered. When only the macroscopic behavior is of interest, a reduced number of modes can be selected, aiming only at training the TANN network within a desired accuracy. If the microscopic fields are the primary objective, the whole procedure can be used as a reduced order modeling tool, and the number of POD modes can be selected to reduce the reconstruction error of the microscopic fields below a given tolerance.

The effectiveness of the methodology is demonstrated through three applications of increasing complexity. These include the homogenization of two inelastic RUCs with continuous microstructure, featuring inclusions of increasing complexity. Furthermore, a complex three-dimensional geotechnical model of a monopile in a clay layer subjected to horizontal loading is studied to demonstrate the applicability of the procedure for the derivation of macroelements.

In all cases, the trained network was able to reproduce accurately the stress-strain (or force-displacement) paths both within and outside the training range. Furthermore, the reconstructed microscopic fields are presented, specifying the reconstruction error as a function of the selected number of POD modes.

Throughout the paper, a loss function that excludes energy terms was used for training the energy network (see Section 3.3). The effectiveness of this function is demonstrated in the application section. By omitting energy terms, the procedure becomes applicable to data from various sources, such

as experimental data, where energy measurements are challenging to obtain.

Despite the linear nature of the dimensionality reduction method, the resulting compression ratios - defined as $CR = 1 - \dim(\mathbf{Z})/\dim(\mathbf{\xi})\%$ - are highly satisfactory, consistently exceeding 90%. Notably, for RUCs with ellipsoidal and leaf-shaped inclusions, IC sets encompassing approximately 100000 degrees of freedom are reduced to an ISV vector with only 25 components, yielding a CR of 99.97%. This high compression ratio significantly reduces the complexity of the hidden layers in the TANN energy network. In the examples considered, a network with a single hidden layer of 100 neurons was sufficient. In most cases, training converged rapidly, typically after 1000 epochs of optimization. The entire procedure requires approximately five minutes of runtime on standard 64-bit machines with 4 cores. Thus, the method is not only accurate but also highly efficient. The macroscopic stress predictions generated by this methodology have a mean absolute error on the order of $1e-4$.

The proposed POD-TANN approach may also serve as a valuable preliminary analysis tool for materials with more complex microstructures. This is particularly relevant for materials exhibiting strong nonlinearities, such as those undergoing softening, where localization phenomena within the RUC can take place. In such cases, classical homogenization techniques, like Asymptotic Expansion Homogenization, typically fail to account for bifurcation or localization phenomena, limiting their applicability in the presence of these complex behaviors.

The challenge with strong nonlinearities lies in the absence of a general homogenization framework that can accurately handle such cases. While AEH provides a rigorous approach for homogenizing periodic microstructures, its formulation does not allow the inclusion of bifurcation phenomena. This limitation prevents its direct application in scenarios where localization occurs, as it is inherently restricted to smooth solutions within a standard continuum framework.

However, the TANN formulation, as presented here, is not tied exclusively to AEH or any specific homogenization technique. This opens the door for alternative frameworks to be considered. Importantly, the TANN methodology for homogeneous materials is not restricted to Cauchy continua, as demonstrated in previous work, [7]. Therefore, if a robust homogenization framework capable of accounting for bifurcation phenomena were developed, particularly one based on higher-order continuum theories, the proposed POD-TANN workflow could be applied.

Such a framework would enable the TANN to model more complex microstructures and material behaviors, including those influenced by localization and bifurcation, thereby broadening the scope of the approach.

5.1. Frontiers on the reconstruction task

An important aspect in the reconstruction of microscopic fields is the fulfillment of boundary conditions.

In the presented examples on periodic RUCs, the POD-TANN approach, while effective in reducing the dimensionality of the system and training efficient models, does not inherently guarantee the enforcement of periodic BCs in decoding. This limitation can introduce reconstruction errors, which depend on the quantity of interest and the various sources of error within the process.

More specifically, in cases where the primary goal is to reconstruct the strain field, the error in fulfilling periodic BCs tends to be directly related to the number of retained POD modes. Since the macroscopic strain is an input to the TANN (for strain-driven formulations), any mismatch between the predicted macroscopic strain and the microscopic strain field reconstruction will affect the overall periodicity. As such, the error will generally decrease as more POD modes are incorporated, ensuring a more accurate representation of the microscopic behavior. This relationship suggests the possibility of developing a POD mode selection criterion explicitly based on the error associated with periodic BC reconstruction. This could complement or even extend the energy-based selection criterion currently used for internal state variable (ISV) selection, allowing for a more tailored approach depending on whether accuracy in boundary condition fulfillment is prioritized. This goes to direction of applying PINNs losses for the resolution of BVPs, see, e.g., [43] or [44].

A key consideration here is that the reconstruction of microscopic stress fields is not directly governed by the macroscopic stress predictions from the TANN, as no explicit localization operator maps the macroscopic stress to its microscopic counterpart. Instead, the microscopic stress field is indirectly reconstructed through the strain field and the internal coordinates. Once the microscopic strain field and ISVs are accurately reconstructed, the stress can be computed using the microscopic constitutive laws of the material (always known in numerical examples, but possibly unknown for more general scenarios). This sequential process introduces additional error sources, particularly when periodic boundary conditions are involved, as any inaccuracy in the

strain field reconstruction could propagate into the stress field. Therefore, ensuring the periodicity of the reconstructed strain field becomes crucial for minimizing errors in the subsequent stress field calculations.

Moreover, the complexity of accurately reconstructing the periodicity in fields such as strain or stress depends not only on the number of POD modes but also on the nature of the microstructure and the loading conditions. In systems with strong heterogeneities or non-linear behaviors, this error may grow, necessitating more sophisticated selection strategies or even hybrid approaches that combine linear reduction methods (such as POD) with non-linear techniques to capture more complex interactions at the micro-scale. By linking the number of POD modes directly to the fulfillment of boundary conditions, this could allow for a more nuanced trade-off between computational efficiency and reconstruction accuracy, especially in scenarios where enforcing periodicity is critical to the validity of the simulation.

In this view, a further advantage of the proposed procedure is its extensibility. The dimensionality reduction achieved through POD is linear and, in cases where the microstructure exhibits strong nonlinearities, may not yield a sufficiently small-dimensional ISV vector at the macroscale (irreducibility). To address this, nonlinear dimensionality reduction methods can be employed to further encode the POD-reduced set. For instance, POD can be used in conjunction with nonlinear autoencoders and SINDy, as demonstrated in [45] and [46]. Additionally, multiple local reduced-order bases (ROBs) can be utilized to manage non-reducible problems by decomposing them into multiple reducible ones, aided by physics-informed cluster analysis (see [47] and [48]).

5.1.1. Frontiers on the macroelement derivation and use

The developed technique demonstrates significant potential in reconstructing the structural field, particularly in the context of macroelement derivation. The ability to accurately reconstruct microscopic fields from macroscopic ISVs, as shown in the monopile example, underscores the practical utility of this methodology for engineering applications. By integrating POD and TANN, a robust and efficient framework is provided for both homogenization and localization, enhancing its applicability to complex geotechnical systems.

However, as highlighted in Section 4.3.4, the "re-usability" of macroelements is currently limited due to the specificity of the computational setup, which is tailored to individual scenarios. This restriction necessitates retraining and reconfiguration when adapting to new conditions, such as changes

in geometry, material properties, or boundary conditions. In this regard, Transfer Learning (TL) emerges as a promising avenue to overcome these limitations. By enabling the fine-tuning of pre-trained networks with smaller datasets, TL could extend the adaptability of macroelements across different scenarios, reducing the computational effort and enhancing the method's scalability.

While the current framework is already effective for specific cases, the integration of TL presents a frontier for further expanding the flexibility and efficiency of the macroelement derivation process. This could enable the use of a generalized parametric macroelement model capable of adjusting to varying conditions, thereby broadening the application scope of the POD-TANN approach in geotechnical engineering.

Overall, the proposed methodology provides a powerful tool for researchers and practitioners in material science and engineering, offering thermodynamic consistency of the predicted system response based on TANN and the flexibility and power of model reduction offered by POD. Thus, the proposed POD-TANN approach shows high potential for modeling heterogeneous inelastic microstructured systems from data and predicting their response. For the class of applications shown, the results are very satisfactory and open the way for modeling even more complex scenarios.

6. Acknowledgment

The authors gratefully thank the funding of the European Research Council (ERC) under the Horizon 2020 research and innovation program of the European Union (Grant agreement ID 757848 CoQuake). In addition, the authors would like to thank Dr. Filippo Masi for their fruitful discussions, as well as the whole CoQuake research group.

Appendix A: Dimensionality reduction of ICs via POD

Mathematically, the POD allows to write a generic field $\mathbf{a}(\mathbf{x}, t)$ by means of a modal expansion (see, e.g., Lumley [10]):

$$\mathbf{a}(\mathbf{x}, t) = \sum_{k=1}^n c_k(t) \Phi_k(\mathbf{x}) = \Phi(\mathbf{x}) \mathbf{c}(t), \quad (.1)$$

in which the column of Φ , $\Phi_k(\mathbf{x})$, are deterministic time-independent spatial functions (POD modes), modulated by the time-dependent coefficients $c_k(t)$,

collected in the column vector $\mathbf{c}(t)$. The data-driven problem associated to the use of POD, is to find the optimal basis of modes, Φ , from data of \mathbf{a} . In practice, this is achieved exploiting the Singular Value Decomposition (SVD), [12].

In the following, \mathbf{A} is used to denote a generic snapshot matrix, i.e., a collection of column vectors of snapshots of the fields $\mathbf{a}(\mathbf{x}, t)$, at subsequent time instants. The notation in equation .1 is thus transformed into $\mathbf{A} = \Phi \mathbf{C}$, where \mathbf{C} collects the time varying coefficients of each mode, each column associated to a different time instant.

The SVD is a unique matrix decomposition that exists for every complex valued matrix $\mathbf{A} \in \mathbb{C}^{n \times m}$, [12]:

$$\mathbf{A} = \mathbf{U} \mathbf{S} \mathbf{V}^*, \quad (.2)$$

where $\mathbf{U} \in \mathbb{C}^{n \times n}$ and $\mathbf{V} \in \mathbb{C}^{m \times m}$ are unitary matrices with orthonormal columns, and $\mathbf{S} \in \mathbb{R}^{n \times m}$ is a matrix with real non-negative entries in the diagonal and zeros elsewhere, with $(*)$ the complex conjugate transpose.

When $n > m$, \mathbf{S} has at most m non-zero elements. The following exact economy representation of \mathbf{A} is therefore possible:

$$\mathbf{A} = \begin{bmatrix} \hat{\mathbf{U}} & \hat{\mathbf{U}}^\perp \end{bmatrix} \begin{bmatrix} \hat{\mathbf{S}} & \mathbf{0} \end{bmatrix}^T \mathbf{V}^* = \hat{\mathbf{U}} \hat{\mathbf{S}} \mathbf{V}^*. \quad (.3)$$

The columns of $\hat{\mathbf{U}}^\perp$ span a vector space that is complementary and orthogonal to that spanned by $\hat{\mathbf{U}}$. The diagonal elements of $\hat{\mathbf{S}}$ are the singular values.

The optimal rank- r approximation to \mathbf{A} , in a least squares sense, is given by the rank- r SVD truncation $\tilde{\mathbf{A}}$, [49]:

$$\tilde{\mathbf{A}} = \tilde{\mathbf{U}} \tilde{\mathbf{S}} \tilde{\mathbf{V}}^* = \inf_{\hat{\mathbf{A}}: \text{rank}(\hat{\mathbf{A}})=r} \|\mathbf{A} - \hat{\mathbf{A}}\|_F. \quad (.4)$$

In the above equation, $\tilde{\mathbf{U}}$ and $\tilde{\mathbf{V}}$ denote the first r leading columns of \mathbf{U} and \mathbf{V} , and $\tilde{\mathbf{S}}$ contains the leading $r \times r$ sub-block of \mathbf{S} , $\|\bullet\|_F$ is the Frobenius norm. For a given rank r , there is no better approximation for \mathbf{A} , in the ℓ_2 sense, than the truncated SVD approximation, $\tilde{\mathbf{A}}$.

In the POD-TANN approach, the generic field \mathbf{a} is specialized to the field of Internal Coordinates, ξ , and the snapshot matrix \mathbf{A} into Ξ . Since the POD modes are time-invariant, the time-varying POD coefficients of the low-rank approximation of ξ may be used as a surrogate variable for tracking

the irreversibility in the system. Thus, the low-rank SVD decomposition of Ξ , $\tilde{\Xi} = \tilde{U}\tilde{S}\tilde{V}^*$, is exploited to identify the time-varying reduced order state variables of the macro-system, $\mathbf{C} \equiv \mathbf{Z}$:

$$\Xi \approx \tilde{\Xi} = \tilde{U}\tilde{S}\tilde{V}^* = \Phi\mathbf{Z} \rightarrow \begin{cases} \Phi = \tilde{U}, \\ \mathbf{Z} = \tilde{S}\tilde{V}^* = \tilde{U}^*\tilde{\Xi}. \end{cases} \quad (.5)$$

The matrix \mathbf{Z} collects the time-varying POD coefficients describing the influence of each POD mode at the considered instant of time. The columns of \mathbf{Z} , \mathbf{z} can thus be interpreted as the ISV vectors at the subsequent time instants.

References

- [1] M. Raissi, P. Perdikaris, G. E. Karniadakis, Physics-informed neural networks: A deep learning framework for solving forward and inverse problems involving nonlinear partial differential equations, *Journal of Computational physics* 378 (2019) 686–707.
- [2] R. Ibanez, E. Abisset-Chavanne, J. V. Aguado, D. Gonzalez, E. Cueto, F. Chinesta, A manifold learning approach to data-driven computational elasticity and inelasticity, *Archives of Computational Methods in Engineering* 25 (2018) 47–57.
- [3] E. Cueto, F. Chinesta, Thermodynamics of learning physical phenomena, *arXiv preprint arXiv:2207.12749* (2022).
- [4] M. Flaschel, S. Kumar, L. De Lorenzis, Automated discovery of generalized standard material models with euclid, *Computer Methods in Applied Mechanics and Engineering* 405 (2023) 115867.
- [5] F. Rocha, S. Deparis, P. Antolin, A. Buffa, Deepbnd: a machine learning approach to enhance multiscale solid mechanics, *Journal of Computational Physics* (2023) 111996.
- [6] M. Yin, E. Zhang, Y. Yu, G. E. Karniadakis, Interfacing finite elements with deep neural operators for fast multiscale modeling of mechanics problems, *Computer Methods in Applied Mechanics and Engineering* 402 (2022) 115027.

- [7] F. Masi, I. Stefanou, P. Vannucci, V. Maffi-Berthier, Thermodynamics-based artificial neural networks for constitutive modeling, *Journal of the Mechanics and Physics of Solids* 147 (2021) 104277. doi:<https://doi.org/10.1016/j.jmps.2020.104277>.
- [8] F. Masi, I. Stefanou, Multiscale modeling of inelastic materials with thermodynamics-based artificial neural networks (tann), *Computer Methods in Applied Mechanics and Engineering* 398 (2022) 115190. doi:<https://doi.org/10.1016/j.cma.2022.115190>.
- [9] F. Masi, I. Stefanou, Evolution tann and the identification of internal variables and evolution equations in solid mechanics, *Journal of the Mechanics and Physics of Solids* 174 (2023) 105245. doi:<https://doi.org/10.1016/j.jmps.2023.105245>.
- [10] J. L. Lumley, The structure of inhomogeneous turbulent flows, *Atmospheric turbulence and radio wave propagation* (1967) 166–178.
- [11] P. Holmes, J. L. Lumley, G. Berkooz, C. W. Rowley, *Turbulence, coherent structures, dynamical systems and symmetry*, Cambridge university press, 2012.
- [12] S. L. Brunton, J. N. Kutz, *Data-driven science and engineering: Machine learning, dynamical systems, and control*, Cambridge University Press, 2022.
- [13] R. Sampaio, C. Soize, Remarks on the efficiency of pod for model reduction in non-linear dynamics of continuous elastic systems, *International Journal for numerical methods in Engineering* 72 (1) (2007) 22–45.
- [14] G. Kerschen, J.-C. Golinval, Physical interpretation of the proper orthogonal modes using the singular value decomposition, *Journal of Sound and vibration* 249 (5) (2002) 849–865.
- [15] J.-C. Michel, P. Suquet, Nonuniform transformation field analysis, *International journal of solids and structures* 40 (25) (2003) 6937–6955.
- [16] J. Michel, P. Suquet, Computational analysis of nonlinear composite structures using the nonuniform transformation field analysis, *Computer*

- Methods in Applied Mechanics and Engineering 193 (48) (2004) 5477–5502, advances in Computational Plasticity. doi:<https://doi.org/10.1016/j.cma.2003.12.071>.
- [17] J.-C. Michel, P. Suquet, Non-uniform transformation field analysis: a reduced model for multiscale non-linear problems in solid mechanics, in: Multiscale Modeling In Solid Mechanics: Computational Approaches, World Scientific, 2010, pp. 159–206.
 - [18] J.-C. Michel, P. Suquet, A model-reduction approach in micromechanics of materials preserving the variational structure of constitutive relations, Journal of the Mechanics and Physics of Solids 90 (2016) 254–285. doi: <https://doi.org/10.1016/j.jmps.2016.02.005>.
 - [19] G. J. Dvorak, Transformation field analysis of inelastic composite materials, Proceedings: Mathematical and Physical Sciences 437 (1900) (1992) 311–327.
 - [20] B. Halphen, Q. S. Nguyen, Sur les matériaux standard généralisés, Journal de mécanique 14 (1) (1975) 39–63.
 - [21] P.-M. Suquet, Local and global aspects in the mathematical theory of plasticity, Plasticity today (1985) 279–309.
 - [22] B. D. Coleman, M. E. Gurtin, Thermodynamics with internal state variables, Journal of Chemical Physics 47 (1967) 597–613.
 - [23] W. Muschik, Survey of some branches of thermodynamics, Journal of Non-equilibrium Thermodynamics - J NON-EQUIL THERMODYN 33 (2008) 165–198. doi:10.1515/JNETDY.2008.008.
 - [24] C. Miehe, Strain-driven homogenization of inelastic microstructures and composites based on an incremental variational formulation, International Journal for numerical methods in engineering 55 (11) (2002) 1285–1322.
 - [25] J. Pinho da Cruz, J. Oliveira, F. Teixeira Dias, Asymptotic homogenisation in linear elasticity. part i: Mathematical formulation and finite element modelling, Computational Materials Science 45 (4) (2009) 1073–1080. doi:<https://doi.org/10.1016/j.commatsci.2009.02.025>.

- [26] N. S. Bakhvalov, G. Panasenko, Homogenisation: averaging processes in periodic media: mathematical problems in the mechanics of composite materials, Vol. 36, Springer Science & Business Media, 2012.
- [27] A. Galli, et al., Macroelement approaches for geotechnical problems: a promising design frame-work, *Rivista Italiana di Geotecnica* 54 (2) (2020) 27–49.
- [28] A. G. Baydin, B. A. Pearlmutter, A. A. Radul, J. M. Siskind, Automatic differentiation in machine learning: a survey, *Journal of Machine Learning Research* 18 (2018) 1–43.
- [29] S. Fresca, A. Manzoni, Pod-dl-rom: Enhancing deep learning-based reduced order models for nonlinear parametrized pdes by proper orthogonal decomposition, *Computer Methods in Applied Mechanics and Engineering* 388 (2022) 114181.
- [30] M. Gavish, D. L. Donoho, The optimal hard threshold for singular values is $4/\sqrt{3}$, *IEEE Transactions on Information Theory* 60 (8) (2014) 5040–5053.
- [31] X. He, J.-S. Chen, Thermodynamically consistent machine-learned internal state variable approach for data-driven modeling of path-dependent materials, *Computer Methods in Applied Mechanics and Engineering* 402 (2022) 115348.
- [32] I. Collins, G. Houlsby, Application of thermomechanical principles to the modelling of geotechnical materials, *Proceedings of the Royal Society of London. Series A: Mathematical, Physical and Engineering Sciences* 453 (1964) (1997) 1975–2001.
- [33] M. Smith, ABAQUS Standard User’s Manual, Version 6.9, Dassault Systèmes Simulia Corp, United States, 2009.
- [34] D. Timothy, Incorporating nesterov momentum into adam, *Natural Hazards* 3 (2) (2016) 437–453.
- [35] X. Glorot, Y. Bengio, Understanding the difficulty of training deep feed-forward neural networks, in: *Proceedings of the thirteenth international conference on artificial intelligence and statistics, JMLR Workshop and Conference Proceedings*, 2010, pp. 249–256.

- [36] R. E. Jones, A. L. Frankel, K. Johnson, A neural ordinary differential equation framework for modeling inelastic stress response via internal state variables, *Journal of Machine Learning for Modeling and Computing* 3 (3) (2022).
- [37] H. Matlock, Correlation for design of laterally loaded piles in soft clay, in: *Offshore technology conference, OTC*, 1970, pp. OTC-1204.
- [38] J. M. Mayoral, J. M. Pestana, R. B. Seed, Determination of multidirectional py curves for soft clays, *Geotechnical testing journal* 28 (3) (2005) 253–263.
- [39] G. Yang, B. Bai, A thermodynamic model to simulate the thermo-mechanical behavior of fine-grained gassy soil, *Bulletin of Engineering Geology and the Environment* 79 (2020) 2325–2339.
- [40] D. N. Gorini, L. Callisto, A multiaxial inertial macroelement for deep foundations, *Computers and Geotechnics* 155 (2023) 105222.
- [41] T. Qu, J. Zhao, S. Guan, Y. Feng, Data-driven multiscale modelling of granular materials via knowledge transfer and sharing, *International Journal of Plasticity* 171 (2023) 103786.
- [42] S. Zhang, L. Ding, M. Xie, X. He, R. Yang, C. Tong, Reliability analysis of slope stability by neural network (nn), principal component analysis (pca), and transfer learning (tl) techniques, *Journal of Rock Mechanics and Geotechnical Engineering* (2023).
- [43] D.-V. Nguyen, M. Jebahi, F. Chinesta, Spatio-temporal physics-informed neural networks to solve boundary value problems for classical and gradient-enhanced continua, *Mechanics of Materials* (2024) 105141.
- [44] F. Masi, I. Einav, Neural integration for constitutive equations using small data, *Computer Methods in Applied Mechanics and Engineering* 420 (2024) 116698.
- [45] P. Conti, J. Kneifl, A. Manzoni, A. Frangi, J. Fehr, S. L. Brunton, J. N. Kutz, Veni, vindi, vici: a variational reduced-order modeling framework with uncertainty quantification, *arXiv preprint arXiv:2405.20905* (2024).

- [46] P. Conti, G. Gobat, S. Fresca, A. Manzoni, A. Frangi, Reduced order modeling of parametrized systems through autoencoders and sindy approach: continuation of periodic solutions, arXiv preprint arXiv:2211.06786 (2022).
- [47] S. L. Brunton, J. L. Proctor, J. N. Kutz, Discovering governing equations from data by sparse identification of nonlinear dynamical systems, *Proceedings of the national academy of sciences* 113 (15) (2016) 3932–3937.
- [48] T. Daniel, F. Casenave, N. Akkari, A. Ketata, D. Ryckelynck, Physics-informed cluster analysis and a priori efficiency criterion for the construction of local reduced-order bases, *Journal of Computational Physics* 458 (2022) 111120.
- [49] C. Eckart, G. Young, The approximation of one matrix by another of lower rank, *Psychometrika* 1 (3) (1936) 211–218.